non-peer reviewed preprint submitted to EarthArXiv

A Novel Methodology to Map Hydrogen Storage Potential in Salt Caverns: A Case Study of the Midwestern and Appalachian Regions of the United States

Les G. Armstrong[1], Bradford H. Hager[2], Sarah Coyle[2], Kristin D. Bergmann[2], Caitlin Fukumoto[3],Dharik Mallapragada[1*]

[1]Massachusetts Institute of Technology Energy Initiative, Cambridge, MA
[2]Massachusetts Institute of Technology Department of Earth, Atmospheric, and Planetary Sciences, Cambridge, MA
[3]Massachusetts Institute of Technology Department of Urban Studies and Planning, Cambridge, MA

Corresponding author: *Dharik S. Mallapragada, `dharik@mit.edu`

Abstract

Hydrogen is widely understood to be critical for decarbonizing hard-to-abate sectors like heavy industry, and long-distance transportation as well as balancing a variable renewable energy dominated power grid. Here, we propose a methodology for evaluating the potential for hydrogen storage in geological salt resources. This methodology starts with a characterization of salt resources by considering salt purity and interbedded non-salt lithologies. We then develop a physical model to estimate the storage potential of a cavern, accounting for cavern shape and considering both brittle and ductile failures. We then factor in environmental and safety considerations to develop above-ground exclusion zones. We illustrate this methodology through an assessment of the hydrogen storage potential in the Midwestern and Appalachian regions in the United States. Our results show that the Michigan and Appalachian Salina basins are promising locations for hydrogen storage in salt caverns with a total technical working gas storage potential in Michigan of 2.1×10^9 metric tons of H_2 or 69.9 PWh and 1.3×10^8 metric tons of H_2 or 4.4 PWh in Appalachia. After applying a coarse techno-economic filter, the storage potential of the remaining high value targets is $9.7{\times}10^8$ metric tons of H_2 or 32.4 PWh in Michigan and 1.6×10^7 metric tons of H_2 or 0.54 PWh in the Appalachian region. These insights can be used to further study the value of these resources for regional decarbonization, while the developed methodology can be readily applied to characterize resource potential in other regions.

1 Introduction

Economy-wide decarbonization efforts are expected to heavily rely on wind and solar-based electricity generation to reduce emissions from the electric power sector – for example, the International Energy Agency (IEA) net-zero by 2050 scenario projects wind and solar to provide 70% of total electricity generation by 2050 (International Energy Agency, 2021). This transformation of the supply side needs to be accompanied by changes in final energy consumption that involve displacing fossil fuels via the following approaches: a) increasing use of electricity in final energy, such as via adoption of electric vehicles and heat pumps for building heating and b) in sectors where direct electrification is impractical today, use of alternative energy vectors like hydrogen or hydrogen-derived fuels that are produced in a low-carbon manner, such as using low-carbon electricity (International Energy Agency, 2021). Collectively, all of these drivers are expected to increase the spatial and temporal variability in primary energy supply and final energy demand. This creates incentives to deploy enabling technologies that can support supply-demand balancing through their flexible operation, such as energy storage, transmission and flexible generation technologies.

The role of energy storage in today's fossil-fuel dominant energy system, manifests primarily as pumped hydropower storage in the power sector as well as storage of petroleum and natural gas (NG) in geological formations to balance seasonal variations in demand for these fuels across the economy. In particular, the seasonality of NG demand for heating in the building sector and its use in the power sector to complement VRE generation, is enabled by an extensive pipeline infrastructure as well as underground storage of NG. For instance, the total working gas capacity of underground NG storage in the U.S. was 4790 billion cubic feet (1.443 PWh), or approximately 15% of total consumption of NG in 2022(U.S. Energy Information Administration (EIA), 2024). With declining costs, there is growing interest to deploy Li-ion storage to support increasing deployment of VRE generation in the power sector, as evident from the 680 GW of both standalone and hybrid battery storage projects in the interconnection queue across the U.S as of Dec 2022 (Rand et al., 2021). Based on its high round-trip efficiency (85%), and energy and power capital cost attributes, Li-ion storage is likely to be cost-effective for managing short-duration fluctuations in energy supply and demand, such as over a day. However, their use for longer-duration energy storage is challenged by their relatively high energy capacity costs, even considering the most optimistic future cost projections (Denholm et al., 2023). H_2 has the potential to achieve very low energy capital cost and uniquely exploit additional revenue streams due to the value of the underlying storage medium as a fuel and feedstock in other end-use sectors. Recent studies have highlighted the complementary nature of long-duration energy storage and short-duration storage, such as Li-ion, under scenarios of deeply decarbonized H_2 power grids and the importance of capital cost of energy storage capacity ($/kWh) in the adoption of long-duration storage options like H_2 (Albertus et al., 2020; Jenkins & Sepulveda, 2021; Sepulveda et al., 2021; Bødal et al., 2020). Among options for H_2 based energy storage, geological storage, where available, has the potential to offer the lowest costs of energy storage at $5/kWh (Papadias & Ahluwalia, 2021) as well as scalability to provide GWh-level of storage.

Among the alternative geological sites used for gas storage today, salt caverns have several favorable attributes for H_2 storage; First, salt caverns can cycle through injection and withdrawal of hydrogen gas more quickly than depleted oil and gas fields or aquifers (Sainz-Garcia et al., 2017). This makes them valuable to manage fluctuations in supply and demand (Matos et al., 2019). Second, the relatively low permeability and inert properties of salt reduce leakage and chemical reactions with the H_2 (Tarkowski et al., 2021). Third, compared to aquifers and depleted fields, salt caverns tend to have lower cushion gas requirements. Cushion gas is the minimal amount of gas that must always stay in the cavern to assure stability and results in a capital cost for the facility. In contrast, the working gas is the gas that can be extracted and utilized for practical purposes (Crotogino, 2016). Fourth, there is extensive understanding of the structural integrity and development of salt caverns (Zivar et al., 2021). As of 2022, salt caverns accounted for 10.2% of the underground NG working gas storage capacity in U.S. or 143 TWh (U.S. Energy Information Administration (EIA), 2024) and there are currently four active commercially successful salt cavern H_2 storage sites in the US and in the UK (Panfilov, 2016).

The wide availability of literature related to natural gas geological storage can be leveraged for H_2 salt cavern storage analysis. However, understanding the differences between methane and H_2 such as the size of the molecules, the compressibility factors, and the biochemical and microbial reactions with the surrounding lithologies are critical to studying the potential of hydrogen storage in these formations (Zivar et al., 2021). Caglayan et al. investigated the European context and found a potential 23.2 PWh of H_2 onshore hydrogen storage in salt caverns. This study aims to build on their methodology by addressing the following three areas: a) justifying and expanding upon simplified and generalized assumptions for quantifying the H_2 storage capacity in salt deposits; b) taking into consideration large impure interlayers in salt formations as critical constraints to cavern construction; and c) conducting an analysis of H_2 storage in salt caverns within the U.S. context which considers the construction of new caverns, as opposed to repurposing existing NG storage, as done by Lackey et al. (2023). For this, we develop a physical modeling basis for characterizing H_2 storage in salt deposits that considers locational-specific geological attributes as well as cavern geophysics and geometry.

The novelty of our model is that it considers caverns of variable shapes and sizes that are adjusted based on the physical constraints attributed to the salt layer properties. This flexibility departs from other literature, which commonly considers a "one-size-fits-all" approach to cavern design (Caglayan et al., 2020; Lord et al., 2014; Ozarslan, 2012). Our approach therefore allows us to account for the specific depth and thickness of salts in each region when designing our caverns, leading to a more accurate calculation of the storable H_2 at a specific location, drawing from the approaches from Williams et al. (2022) and Ślizowski et al. (2017). This can provide a basis for the many heuristics suggested for designing H_2 storage caverns in salts that are cited in the literature such as optimal depth for cavern construction.

We then apply the above model to the case study of the salts in Michigan and Appalachian regions to quantify the potential for H_2 storage in this region after accounting for geological resource constraint and above-ground land use constraints. Our findings reveal that the total overall technical working gas storage potential in Michigan is 2.09×10^9 metric tons of H_2 or 69.90 PWh (1 PWh =1000 TWh) and 1.32×10^8 metric tons of H_2 or 4.40 PWh in Appalachia. That is, Michigan has roughly 15 times more storage potential than the Appalachian region. After applying filters related to number of caverns and cushion gas requirements that impact commercial viability, these potentials are reduced to 32.36 PWh in the case of Michigan and 0.54 PWh in Appalachia.The relatively thicker and more homogeneous spatial distribution of salts in the Michigan region, characterized by well log data, explains the greater storage potential in this region compared to the Appalachian region. The salt resources of the Appalachian region are generally less homogeneous with the presence of significant interlayers that constrain the potential of cavern construction for hydrogen gas storage. In addition, our mapping of the Michigan resources is more robust than those in Appalachia due to the wider availability of public well log data. Overall, the study provides a systematic basis for evaluating H_2 storage potential in salts in any region subject to the availability of data to characterize the salt resource, which we found to be a key limitation to scale-up our analysis to the national level.

2 Methodology

2.1 Salt Basin Characterization

To accurately assess the potential size and type of caverns that can be constructed for hydrogen storage, a geospatial analysis of salt resources is needed. The goal is to create a dataset that specifies the depth to top salt and thickness of salt resources across large regions but that also has enough granularity to resolve interlayers of non-salt lithologies.

One of the main constraints for hydrogen storage in salt caverns is the availability of high-quality salt basins. The U.S. has extensive salt resources, including bedded salts and salt diapirs. Bedded salts are geological formations of horizontal layers of rock salts. A salt dome is a general term for a domal upwelling that comprises a salt core and its envelope of deformed overburden.

Most research conducted in the US for hydrogen storage in salt caverns has focused on the salt diapers in the Gulf (Duffy et al., 2021; Schuba & Moscardelli, 2023; Abreu et al., 2023), which is where the three active H_2 salt cavern storage facilities in the US operate (Zivar et al., 2021). Moreover, salt diapirs are also utilized to store hydrocarbons such as the Strategic Petroleum Reserve (SPR) (Alessandra Simone et al., 2021). Much less attention has been paid to bedded salts, which are more geographically abundant within the United States (Horváth et al., 2018). Our research is directed toward these latter resources with the goal of broadening our understanding of the potential of these resources in the hydrogen economy.

For bedded salts, it is important to consider the quality of the salts as well as the composition and porosity of the interlayers. Lateral and vertical heterogeneity within salt is related to depositional processes as well as post-depositional deformation. H_2 is a small molecule that can escape through more porous areas (Zhu et al., 2023). Gas escape from salt caverns has been modeled for CO_2 sequestration which has shown that the amount of gas escaped is negligible throughout the cavern life and that it dispersed in the subsurface (Dinescu et al., 2021). However, we could not find such study for H_2, a much smaller molecule that is cyclically injected and withdrawn, resulting in a higher chance of escaping the cavern and leaking into the atmosphere. The escape of H_2 not only has economic impacts, but can also lead to environmental impacts, such as exacerbating the greenhouse gas effects of methane in the atmosphere (Ocko & Hamburg, 2022; Warwick et al., 2023). In addition, contamination due to geochemical (Wang et al., 2015) or microbial reactions with these interlayers is another risk that must be considered and monitored (Dopffel et al., 2023).

2.1.1 Salt layer interpretation

The methodology to create a detailed salt characterization for H_2 storage assessment relies on the analysis of petrophysical well logs to identify the pure layers of salts and interpolating between well logs to create regional maps of thickness and depths of salt resources across each basin. Our work primarily utilizes geophysical well logs, supplemented by deviation and location surveys, production histories, driller's logs including cuttings descriptions, historical driller's reports and existing well log interpretations including lithology and formation tops. Ideally, this well log analysis would be complemented with 3D seismic data, however, this data is not publicly available so we did not include it in our analysis.

Well log data for the Michigan Salina Basin was obtained from the Michigan Geological Repository for Research and Education at Western Michigan University, with approximately 900 wells used for Michigan Basin salt maps (Harrison et al., 2016; Voice et al., 2017). Most of the interpretative work for the Michigan Basin was performed by geologists within these institutions; however, we checked the interpretations for each well log and picks for the base and top of salt-rich intervals. We made corrections to reconcile inconsistencies between previous interpretions.

Well log data for the Appalachian Basin were extracted data from publicly available digitized geophysical well log data and driller tops from six state systems of record to create a single database . State data sources included the Empire State Organized Geologic Information System (ESOGIS), Appalachian Basin Tight Gas Reservoirs Project File Repository, the West Virginia Geological and Economic Survey, the Appalachian Storage Hub (ASH) Project File and Data Search, and the Exploration and Development Wells Information Network (EDWIN). More than 400 wells were imported and their data were imported. After well log quality control, 348 wells were interpreted and used in Appalachian Basin Salt Mapping.

The interpretation process we took for both the Michigan and Appalachian basins involved identifying new formation, member, and lithologic unit tops, or checking the quality of existing tops using geophysical log responses, as these correspond to a combination of changing lithology, mineralogy, and porosity. Lithostratigraphic interpretations were made and used to mark depths of individual salt bed tops and bases. Additionally, geophysical logs were used to estimate halite purity and quality. Isopach thicknesses were calculated for each interpreted evaporite layer, and gridded contour isopach and structure maps were created using Petra software. Depth and thickness criteria were also established for viable salt cavern resources.

In Figure 1 a sample of the Petra software interface can be observed where we show a cross-section of eight well logs cutting across Michigan with their respective evaporite units correlated across the basin. An additional step that is needed to calculate the lithostatic pressure from the depth to top salt involves taking into consideration the variations in elevation across the regions of interest. To do this, we access the USGS publicly available Digital Elevation Maps (DEMs) which supply fine-grained elevation data and then add these values to the depth values which are measured from sea-level based on log well input data. This step is not a large source of error in the maps of the Michigan Basin but it is in the Appalachian Basin, where, in addition to sparser well coverage, the topography varies significantly within short distances, creating significant variability on short-length scales.

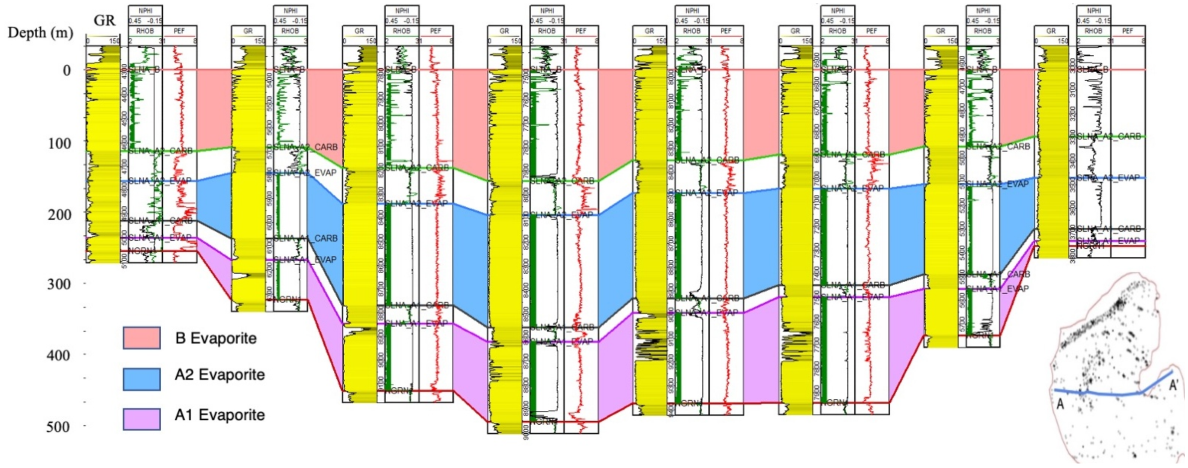

Figure 1. East-west cross-section of the lower Salina in the central Michigan Basin constructed using PETRA. Formation tops for the A-1 (purple), A-2 (blue), and B (pink) Evaporites were manually marked for each log and the formation tops were then interpolated linearly across the basin. The y-axis represents the depth in meters from the top of the B Evaporite, showing the thickness of each salt layer. The measurements shown are the gamma rays (GR, yellow), the density logs (RHOB, green), the neutron porosity (NPM, black), and the photoelectric factors (PEF, red). The bottom right is a map of the wells (black dots) used to constrain the thickness and depth of the A-1, A-2, and B Evaporites of the Michigan Salina Group. The East-West cross-section is represented as the blue line that connects the points A and A'.

2.2 Physical Model

The mass of gas that can be stored in a cavern (S_{stor}) can be derived via the following equation:

$$S_{stor} = \rho_{\max} \times V_{\max} - \rho_{\min} \times V_{\min} \tag{1}$$

For most gas storage in salt reservoirs, that operate via pressure swings, the volume of the cavern, V, does not change significantly during operating cycles. Hence, the gas storage definition can be simplified to be:

$$S_{stor} = (\rho_{max} - \rho_{min}) \times V \tag{2}$$

Here densities $\rho_{\max}$ and $\rho_{\min}$ are determined from pressures $p_{\max}$ and $p_{\min}$ via the equation of state relating density to pressure and temperature discussed in Section 2.2.4[1].

The variable inputs required for the physical model are the depth, thickness, rheological parameters, and temperature of the available salt resources. For the most part, the thickness constrains the available cavern volume, while the depth determines the possible operating pressure range of the cavern. Taking both the volume and the operating pressures into account, we can then calculate the cushion gas, the working gas, and therefore the storable mass of hydrogen.

[1] An important exception is the Teesside H_2 reservoir in the United Kingdom which operates at constant pressure, with the volume of the cavern changing by injection and production of brine(Atkins, 2018).

2.2.1 Cavern Shape and Volume

Most estimates assume that salt caverns for hydrogen storage are vertical cylinders that take advantage of thick salts (+200m), such as those like the Permian-aged Zechstein present in the subsurface across much of Europe (Caglayan et al., 2020; Lankof & Tarkowski, 2020; Stone et al., 2009). However, within our target regions, once the interbedded non-halite layers are considered, the thickness of usable salt layers does not exceed 160 meters, with an average thickness of approximately 70 meters. This indicates that vertical cylinders, commonly utilized in salt diapirs and the thickest bedded salt deposits, would be an inefficient use of space for these comparatively thinner bedded salts. This led us to consider other shapes such as spherical and horizontally oriented cylindrical caverns. We explored the geophysical stability of these different cavern shapes over the lifetime of a cavern. It should be noted that due to difficulties in monitoring and precisely controlling the leaching process during cavern construction, the resulting cavern shapes often deviate from their theoretical shapes (Wang et al., 2013).

Spherical caverns are currently deployed for gas storage in the natural gas storage industry (Horváth et al., 2018; Wang et al., 2019). Figure 2 is a schematic showing a spherical cavern model in a bedded salt formation. The volume of a sphere is:

$$V = \frac{4}{3}\pi \times r^3 \tag{3}$$

Here, V is the volume [m^3] of the cavern and r [m] is the radius of the sphere.

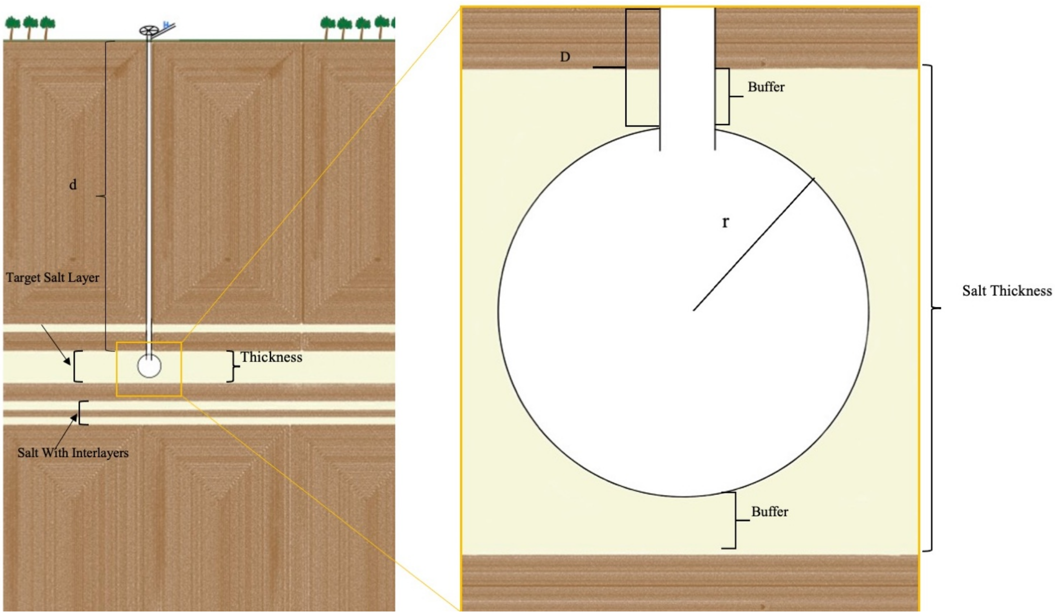

Figure 2. A simplified representation of an example spherical cavern. Here d represents the depth of the surface to the target salt structure, D represents the depth from the surface to the top of the cavern, r represents the radius of the cavern, and the buffer represents the buffer distance of the cavern inside of the salt structure

We also explored the possibility of using horizontal cylindrical shapes for caverns - see Appendix B.

2.2.2 Pressure

Given our assumption that the volume change during a storage cycle is negligible, maximizing the mass injected and extracted requires maximizing $p_{\max}$ and minimizing $p_{\min}$. Determining $p_{\max}$ and $p_{\min}$ requires consideration of the rheological properties of salt as a function of stress and temperature.

If the gas pressure within the cavern is close to or greater than the lithostatic pressure, failure via fracturing of the rock or injection hardware is expected. If the $p_{\max}$ is too high, it may cause cracks in the salts which may lead to the escape of the gas. This sets a limit on the maximum pressure $p_{\max}$ where the top of the cavern, at depth D (Figure 2), is the weak point:

$$p_{\max} < \rho \times g \times D \times c_1 \tag{4}$$

where c_1 is a constant ~ 0.8 (Crotogino, 2022).

If the difference in stress between the gas inside the cavern and the rock mass surrounding the cavern is too large (i. e., the gas pressure is too low compared to the lithostatic pressure of the rock), the cavern will collapse. This sets a limit to the minimum pressure $p_{\min}$. In contrast to the maximum pressure, this limit is at the bottom of the cavern, at a depth of $D+H$, where H is the vertical height of the cavern. For $p_{\min}$ there are two mechanisms that can come into play: brittle failure (Berest & Brouard, 1998), and ductile failure (X. Ma et al., 2021). The limiting value of $p_{\min}$ is the greater of these two relevant pressures explained below:

1. Brittle failure occurs when the internal gas pressure is not large enough to offset the external lithostatic pressure leading to collapse and loss of stability of the cavern. This pressure limit is given by:

$$p_{\text{min\_brittle}} > \rho \times g \times (D + H) \times c_2 \tag{5}$$

   where c_2 is a constant ~ 0.3 (Caglayan et al., 2020).
2. Ductile failure occurs when the internal gas pressure is not large enough to offset the external lithostatic pressure leading to creep failure over long time horizons. The result of this creep is that the cavern slowly fills in over time. Ductile flow of salt is highly dependent on the deviatoric shear stress σ, and less so to the temperature T. The deviatoric strain rate is given by:

$$\dot{\varepsilon} = A \exp\left(\frac{-Q}{RT}\right) \sigma^n \tag{6}$$

   Here R is the gas constant. (Berest & Brouard, 1998; L. Ma et al., 2021; Nye & Mott, 1953). Because the strain rate depends on the shear stress raised to the power n, this is called power law flow. The three parameters A, Q, and n are determined experimentally by measuring $\dot{\varepsilon}$ at multiple values of σ and T and performing a fitting exercise to constrain the parameters. This is experimentally challenging and there are considerable uncertainties in estimates of individual parameters, as well as substantial covariance among estimates. Because the collapse rate of a cavern in the ductile flow regime depends on σ^n and n is typically 4 or more, a critical stress difference σ^* quantifies the conditions for rapid cavern collapse. For ductile creep, the cavern shrinks significantly unless

$$p_{\text{min\_creep}} > \rho \times g \times (D + H) - \sigma^* \tag{7}$$

   where σ^* is on the order of 20 MPa, and depends on the flow properties and temperature of the salt surrounding the cavern (Berest & Brouard, 1998). In Appendix A, the derivation of σ^* and how it relates to $p_{\text{min\_creep}}$ is shown, considering both spherical and horizontal cylinder cavern shapes.

2.2.3 Temperature

The temperature is calculated as a function of depth, based on the assumption of: a) the surface temperature of 17C (290K) representing an average over the year (Fabig & Brückner, 2011) and b) a geothermal gradient of $23\deg C/\text{km}$. The center of the cavern is taken as the point of reference for calculating the temperature as function of depth (where D and H are in metres).

$$T = 290 + 0.023 \times (D + \frac{H}{2}) \tag{8}$$

2.2.4 Non-Ideal Gas Equation

Hydrogen, like most gases, deviates from ideal gas law behavior at high pressures such as in the case for salt cavern storage. To calculate the equations of state, we employ the CoolProp Python package (Bell et al., 2014; Leachman et al., 2009). For our cavern capacity calculations, we ignore dynamic behaviors related to change in cavern volume via creep and thermodynamic interaction of gas injection and withdrawal. In other words, we assume that both the temperature and volume are constant and determined by equations (8) and (3), respectively.

2.2.5 Physical Model Analysis

The physical model allows us to calculate the operating pressures and volume of the caverns based on the input parameters of the depth to the top of the cavern and the thickness of the usable salt, as well as their rheological property values. This in turn also allows us to then calculate the working and cushion gas in the cavern.

Figure 3) plots the maximum and minimum allowable pressures as function of depth for the Salina salts (rheological properties described in Appendix A). We observe a trend of increasing operating pressure range ($P_{max} - P_{min}$) until around 1500 m where this pressure difference once again begins to decrease. At this point, the creep driven critical pressure σ^* is reached leading to the minimum operational pressure being driven by brittle failure rather than ductile failure. This optimal depth "sweet spot" corresponds to the largest operational pressure range and therefore storable working gas.

Other models that also estimate hydrogen storage capacity, such as Caglayan et al., do not explicitly take into consideration the ductile minimum pressure, leading to the alternate finding that increasing depth leads to increasing gas storage. This would in turn suggest that the most valuable salts are the deepest salts. This contradicts heuristics found across the literature that assert that the optimum depth for cavern construction is in between approximately 800 m to 1700 m (Lankof et al., 2022; Michael Susan, 2019; Parkes et al., 2018; Williams et al., 2022; Zheng et al., 2020). One of the main contributions of this paper is that it offers a reasonable description of these heuristics rooted in geophysical models that is relatively easy to implement.

2.3 Geospatial Analysis

With the geospatial data of the available salts in the Michigan and Appalachian basins of Section 2.1 and the physical model detailed in Section 2.2, we can combine both methodologies to calculate the hydrogen storage potential in the Michigan and Appalachian regions.

2.3.1 Spatial Cavern Placement

To rasterize the data, we gridded our results in 500 m x 500 m cells each with their own depth and thickness value. To ensure the tightness of the salt, a 15 m buffer within the evaporite layer is applied both above and below the cavern (totaling 30 m) after which

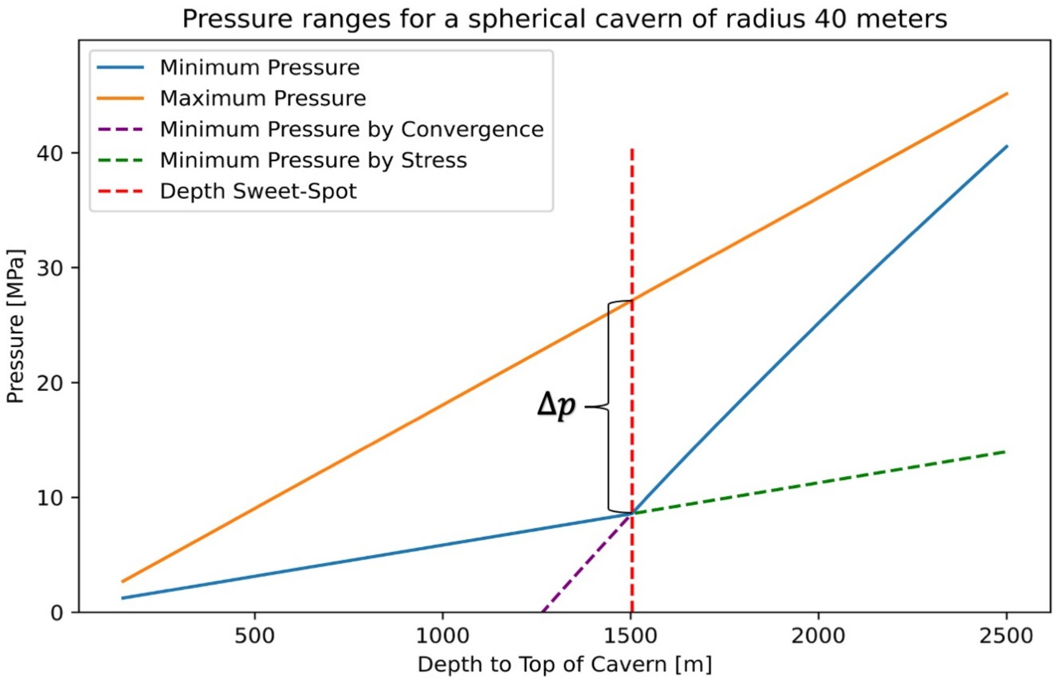

Figure 3. Pressure ranges for a spherical cavern of radius $r = 40\,\mathrm{m}$ for the Salina salts (rheological parameters reported in Appendix A). The depth "sweet spot", corresponding to D = 1500 m and large working gas pressure difference, can be approximated by the intersection of the minimum pressure curves for ductile failure (7)) and brittle failure (Eq (5)). If creep were ignored, Δp would increase with depth as seen by the widening difference between the maximum pressure (orange line) and the minimum pressure by stress (dashed green line).

the remaining thickness can be utilized for cavern construction. Given the variation in bed thicknesses and therefore cavern sizes across the salt basin, multiple caverns are allowed to be constructed in a single 500 m x 500 m grid cell to take full advantage of the resource.

To avoid significant inter-cavern pressure interactions, we follow the available guidance on inter-cavern spacing, from the design of compressed air energy storage caverns (Allen et al., 1982) as well as natural gas storage (Energy Resource Committee of the Interstate Oil and Gas Compact Commission (IOGCC), 1995), which recommend the caverns be placed at a distance of 8 times the radius from their central axis from each other as to prevent critical interactions between cavern pressures. This results in the number of caverns that fit into a single cell to be:

$$N_{\text{caverns\_sphere}} = \frac{\text{Area}}{\pi(4r)^2} \tag{9}$$

The resulting number of caverns in a grid cell may be a noninteger value. It is assumed that these caverns can be distributed across the grid cells in a way that ensures the non-integer values complement each other across cells to form complete caverns. By multiplying this number of caverns by the working gas capacity of a single cavern, we can approximate the total working gas potential of each grid cell.

$$\text{Total working gas in cell} = \text{working gas in a cavern} \times N_{\text{caverns}} \tag{10}$$

2.3.2 Land Exclusion Criteria

Despite the maturity of the salt leaching industry, not all land with salt resources can be utilized for salt cavern storage. There are important environmental and safety factors that must be considered. Salt (halite) is ductile and mobile, which can lead to multiple issues, including cavern convergence, ground subsidence, borehole closure, high-pressure gas and brine pockets, casing collapse, and in extreme cases, cavern collapse, micro-seismicity, and long-term land subsidence issues (Bérest & Brouard, 2003).

For this purpose, following the approach of Caglayan et al. (2020), the open-source model Geospatial Land Availability for Energy Systems (GLAES) tool originally developed by Ryberg et al. (2017) for wind turbine placement was adapted and applied for land exclusion analyses. The land exclusion constraints are shown in Table 1, where a distance buffer is applied based on a review of the literature on underground air compression and natural gas storage technologies (Lux, 2009; Allen et al., 1982). The disposal of brine, which presents a significant environmental concern (Crotogino, 2022), is not explicity considered due to the abundance of USA EPA class II disposal wells in the two regions (Michigan Department of Environment, Great Lakes, and Energy, 2024).

Once all land exclusion constraints have been applied, these 'exclusion maps' are overlayed on the salt resource map that reveals eligible land for cavern construction. The resulting exclusion map for the Michigan and Appalachian regions is shown in Figure 4.

3 Results

3.1 Salt Resources Analysis

Evaporite layer characterization is detailed in the subsections below. The resulting maps for the A-2 Evaporite in the Michigan Basin and the F-4 Evaporite in the Appalachian Basin, the most promising salt layers in each region respectively, is shown in Figure 5. Full characterization of other layers in each basin are reported elsewhere in further detail (?, ?).

Table 1. Exclusion criteria based on different categories and their respective sources.

Criteria	Excluded within	Source
Urban areas	2500 m	2020 U.S. Census populated places (class 6-10)
Rural areas	2000 m	2020 U.S. Census populated places (class 1-5)
Protected areas	200 m	USGS Protected Areas Database (GAP Status 1 & 2)
Water bodies	200 m	USGS National Hydrography Database
Railways and major roads	200 m	U.S. Census Bureau TIGER/Line Files
Pipelines (Fossil Fuels)	200 m	U.S. EIA state maps

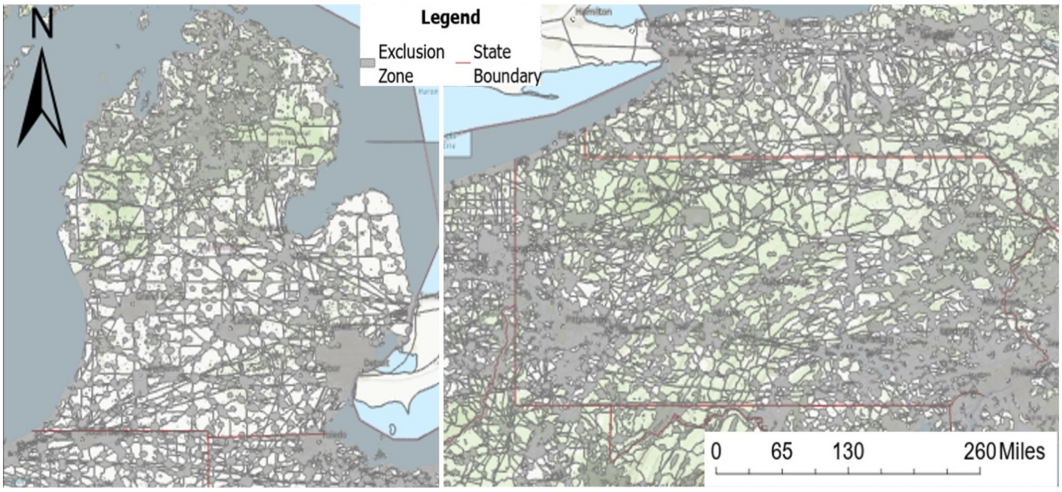

Figure 4. Exclusion maps of the Michigan and Appalachian regions in grey. Criteria for the development of these maps are given in Table 1.

3.1.1 Michigan Salina Basin

The Michigan basin's deepest evaporite layer, the A-1 Evaporite, has a maximum thickness of approximately 143 meters in Bay County, reaching a depth of approximately 2508 meters below sea level. The thickest part of the evaporite is located near the center of the basin in Isabella, Midland, and Bay Counties, while it thins out to the north and south and gradually to the east and west, forming an elongated depocenter that trends southwest to northeast across the basin. In addition, the A-1 Evaporite in the basin contains potash minerals deposited in two distinct beds, which are discussed in detail and shown in map view by W. Harrison III and P. Voice (?, ?).

Overlying the A-1 Evaporite and the A-1 Carbonate (the Ruff Formation), which has a thickness ranging from approximately 15-25 meters, is the A-2 Evaporite. The depth range of the top of the A-2 Evaporite is approximately 415-2364 meters below sea level. The maximum thickness of the A-2 Evaporite is approximately 158 meters, and, like the A-1 Evaporite, it thins to zero thickness at the basin margins. The thickness of the A-2 Evaporite increases in the same direction as the depth, with the top of the A-2 Evaporite being about 143 meters shallower at the basin center than the top of the A-1 Evaporite and approximately 40 meters shallower at the basin margins. The depocenter of the A-2 Evaporite is shifted to the north of the A-1 Evaporite, with the thickest center of the A-2 Evaporite located in Alcona and Iosco counties.

The B Evaporite layer is separated from the A-2 Evaporite by the A-2 Carbonate layer, which has a variable thickness ranging from 18 to 55 meters across the area of in-

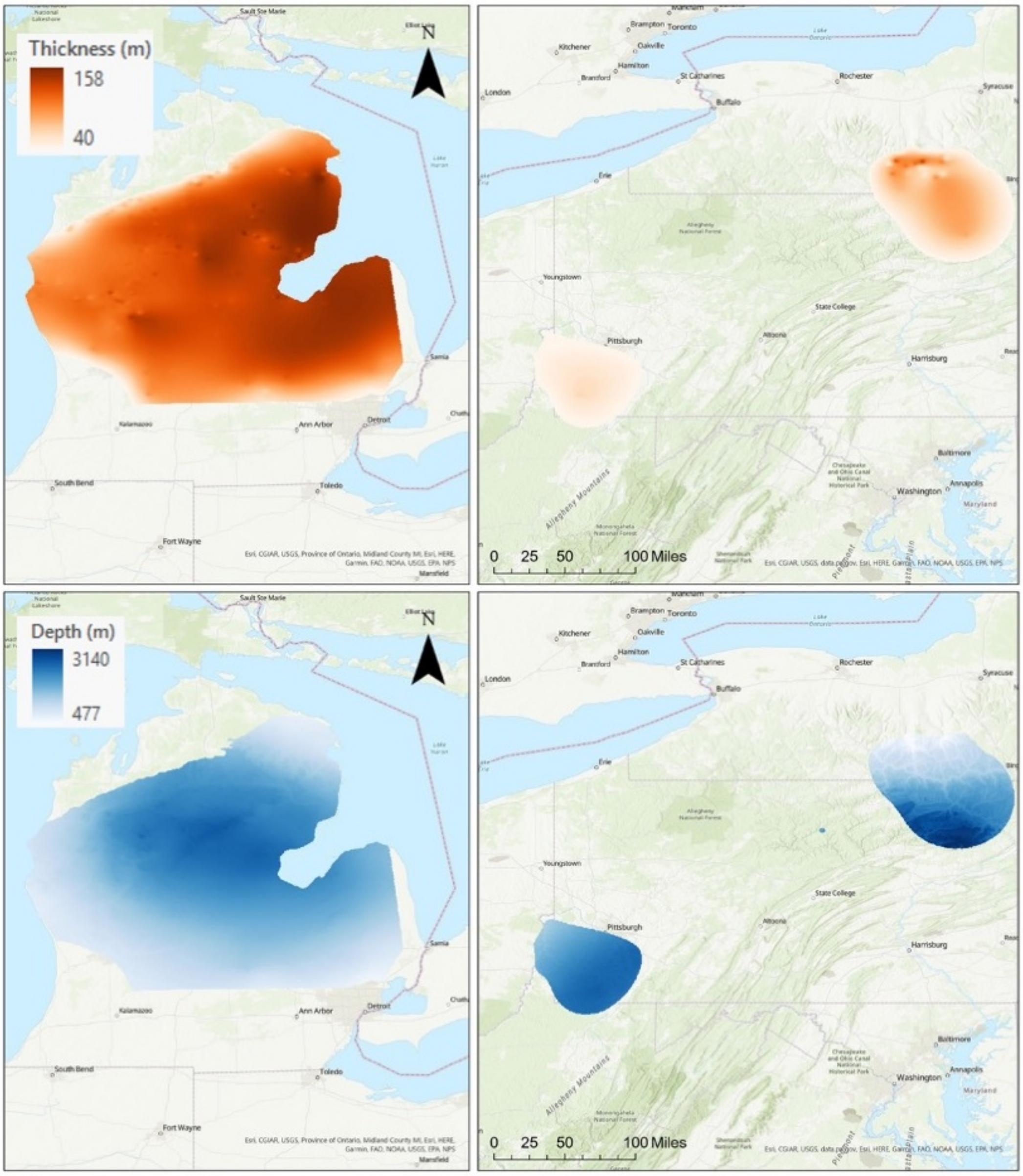

Figure 5. Michigan A-2 (left column) and Appalachian F-4 (right column) Salina Evaporite layer thickness (orange) and depth (blue) to the formation top maps. The thickness reaches up to 158 meters while the depth varies in between 477 meters and 3140 meters

terest. The thickest interval of the A-2 Carbonate layer is found near the basin's center in Bay, Gladwin, and Midland Counties, with a maximum thickness of approximately 160 meters in Bay County. The depth of the top of the B Evaporite layer ranges from 283 to 2176 meters below sea level. At the basin center, the top of the B Evaporite is on average approximately 187 meters shallower than the top of the A-2 Evaporite, and about 131 meters shallower at the basin margins.

Combined, the A and B units in the Michigan basin contain three extensive and continuous evaporite layers, each with a substantial thickness of pure halite that could serve as effective sites for subsurface hydrogen storage. However, local evaluations should be conducted to assess the heterogeneities in the evaporites before creating caverns. The A-1 evaporite's heterogeneities are limited to the basin center, while the A-2 evaporite is the most homogenous, continuous, and thick halite package in the basin.

3.1.2 Appalachian Basin

The Salina A and B units from the Michigan Basin, which are characterized by substantial and pure halite beds, are missing in the Appalachian Basin. In the absence of the A and B units, the F unit become the thickest and most widespread halite within the Appalachian Basin.

The most abundant well penetrations of the Salina Unit F occur in northern Pennsylvania. Nonetheless, data scarcity and low-quality data contribute to significant uncertainty as to whether these penetrations represent a uniform thickening of the salt into northern Pennsylvania or rapid lateral thickness fluctuations. Regional uplift and orogeny during the formation of the Appalachian Mountains distorted the Appalachian basin fill and might have induced significant variations in salt thickness. The extent of this variation cannot be determined without seismic imaging or better well control. The analysis of the Appalachian Basin salts becomes less reliable due to increased deformation, insufficient well control, and the presence of numerous interbeds of porous lithologies and anhydrite within halite-rich intervals, compared to the Michigan Salina Basin salts.

The F-1 Evaporite is the most extensive of the F evaporites. It achieves its greatest thickness in Northern Pennsylvania's Tioga and Bradford counties, peaking at roughly 112 meters in Bradford County. Only two wells penetrate the F-1 Evaporite where the thickness exceeds approximately 53 meters. The remainder of the identified thick F-1 Evaporite region in southern New York and northern Pennsylvania ranges between approximately 30 and 53 meters. The F-1 Evaporite diminishes to zero thickness moving away from the two F-1 Evaporite depocenters towards the basin margins.

Separated from the underlying F-1 Evaporite by a thin layer of carbonates, dolomites, and shales, the F-2 Evaporite is thickest in southern New York and northern Pennsylvania. The most substantial F-2 Evaporite salt intervals sampled by well data, nearly 98 meters thick, are located in New York's Schuyler and Tompkins Counties. Similar to the other F unit evaporite beds, the F-2 Evaporite also has a second depocenter in eastern Ohio and western Pennsylvania; this secondary accumulation does not exceed a thickness of approximately 23 meters. The F-3 Evaporite never surpasses a thickness of 27 meters, rendering it unsuitable for our cavern analysis.

The F-4 Evaporite, being the thickest and purest layer in the F unit, is over 150 meters thick in northern Pennsylvania. In western Pennsylvania and eastern Ohio the F-4 Evaporite is under 61 meters thick within a second depocenter centered in Washington and Green counties in Pennsylvania. The F-4 Evaporite, like the F-1 Evaporite, diminish to zero thickness away from the two F-4 Evaporite depocenters. The topography of the F-4 Evaporite salt structure aligns with the structural contours of the full F unit section and the previously described F evaporites. The F-4 Evaporite reaches its maximum depth in northeastern Pennsylvania, approximately 2438 meters below sea level.

The shallowest F evaporite identified, the F-5 Evaporite, only covers a small area in Tioga County, New York, and Bradford County, Pennsylvania. Similar to the F-3 Evaporite, the F-5 Evaporite does not reach a thickness sufficient for the creation of hydrogen storage caverns and is not discussed further.

The F-4 Evaporite layer is the most promising target for hydrogen storage in the basin. As interpreted from its gamma-ray signature, the most readily available geophysical log data, its homogeneity varies drastically from very clean halite salt in its thickest depocenter to significant interbedded lithologies that could present either solution barriers or thief zones depending on the specific lithology. More detailed constraints on the thickness and quality of the salts come from only a few wells with cored intervals. Significant structural deformation should be considered very likely and related changes in lateral thickness expected. Future work should include characterization using seismic imaging since well log control is limited in much of the most promising regions for salt storage in the F-4 Evaporite. Detailed local studies, targeted exploratory drilling, and careful site assessment should be implemented before further consideration of the F-4 Evaporite for subsurface H_2 storage.

3.2 Geospatial Analysis

By using the physical model for spherical caverns and limiting the results to the availability of determined salt resources within the developed exclusion zone, we can map the potential for hydrogen storage. Figure 6 is a map that depicts the potential for hydrogen storage in spherical caverns in the A-2 Michigan evaporite layer and the F-4 Appalachian evaporite layer. This figure shows that for Michigan the maximum total storable working gas potential in a single 500 m x 500 m grid cell is found in the A-2 Evaporite layer and reaches approximately 11 000 metric tons, or 380 GWh. This amounts to 1.31 caverns of volume 980 000 m^3 with working gas of 8700 metric tons. For Appalachia, the maximum storable working gas in a 500 m x 500 m grid cell is found in the F-4 Evaporite layer and can store approximately 7700 metric tons, or 256 GWh, in 3.74 caverns of volume 200 000 m^3 and working gas 2000 metric tons each.

However, directly comparing the storage capacities of two caverns can be misleading due to the difference in volumes. Larger caverns take more time and are more expensive to develop (Papadias & Ahluwalia, 2021), so utilizing another metric that considers these differences in volumes is preferable (Lankof et al., 2022). Because of this, the energy density is calculated by dividing a cavern's storage potential by its volume. In Figure 6, we show the energy density reaches 398 $\mathrm{kW\,h\,m^{-3}}$ in both the Michigan and Appalachian regions, though Michigan does have a much larger area with this high energy density potential.

Observing this energy density map and comparing it to the Michigan A-2 Evaporite depth map in Figure 5, we can clearly see that there is a ring of high density in the same location as the ring of depth of approximately 1500 m. This reinforces our conclusion of having an optimal depth for cavern construction, especially as the calculation takes into account how much hydrogen can be stored per m^3 of cavern.

3.3 Capacity Analysis

In this subsection we calculate the total hydrogen storage potential in salt caverns in the Michigan and Appalachian regions. Since these layers are vertically separated by only a few hundred meters, the constraint on inter-cavern separation distance leads us to only select one salt layer per grid cell for consideration. Therefore, for every cell of the grid, the salt layer with the highest working gas potential is selected while the others are filtered out.

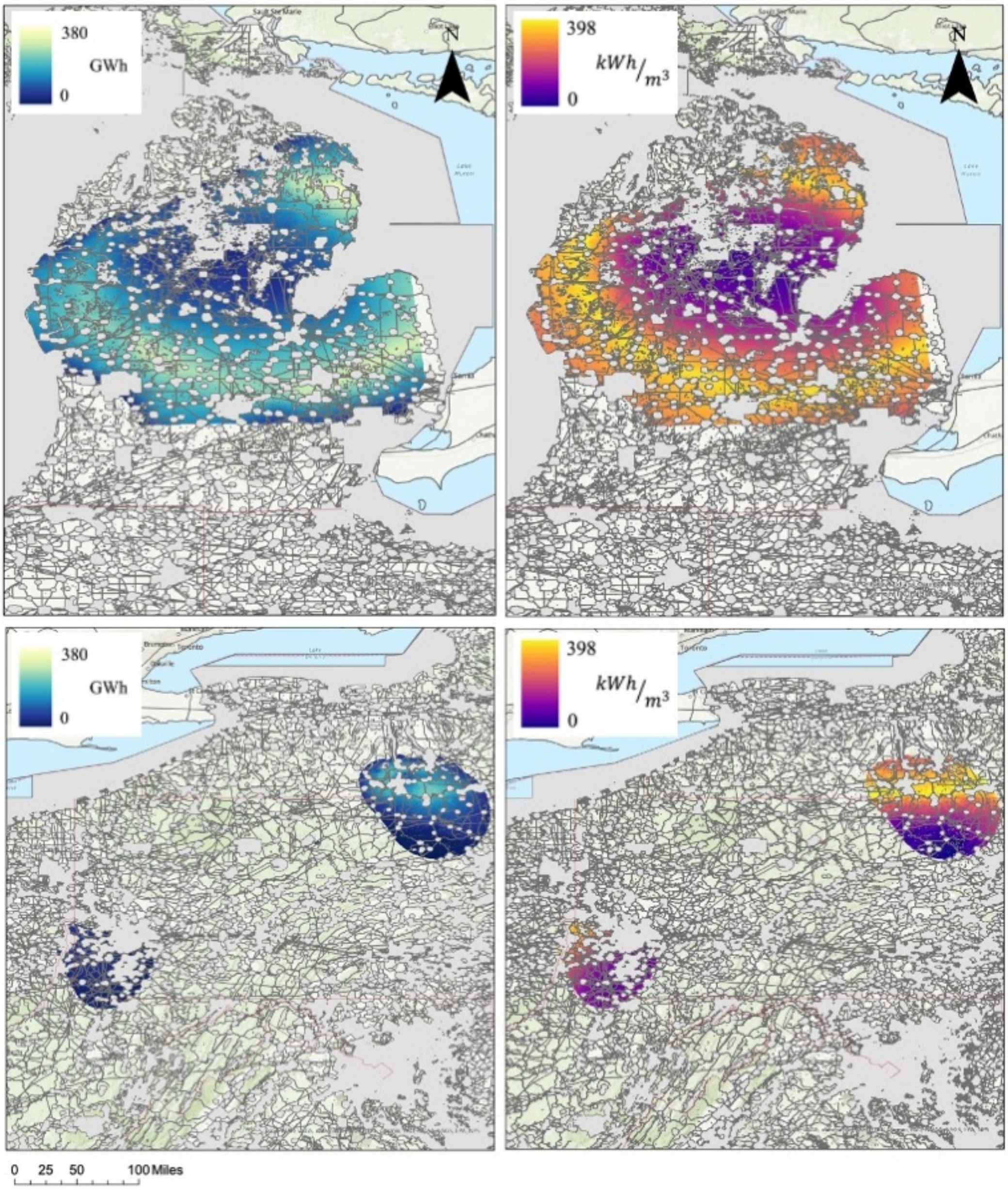

Figure 6. Maps showing the H_2 working gas potential (left column) and energy density (right column) of spherical caverns in the Michigan Salina A-2 Evaporite (top row) and Appalachian Salina F-4 Evaporite (bottom row). Salt layers in 500 m x 500 m grid cells are presented. The working gas reaches up to 380 GWh stored in a single grid cell in the Upper-East corner of the Lower Peninsula of Michigan. The Michigan A-2 Evaporite layer has overall better salt resources than the Appalachian Salina F-4 Evaporite.

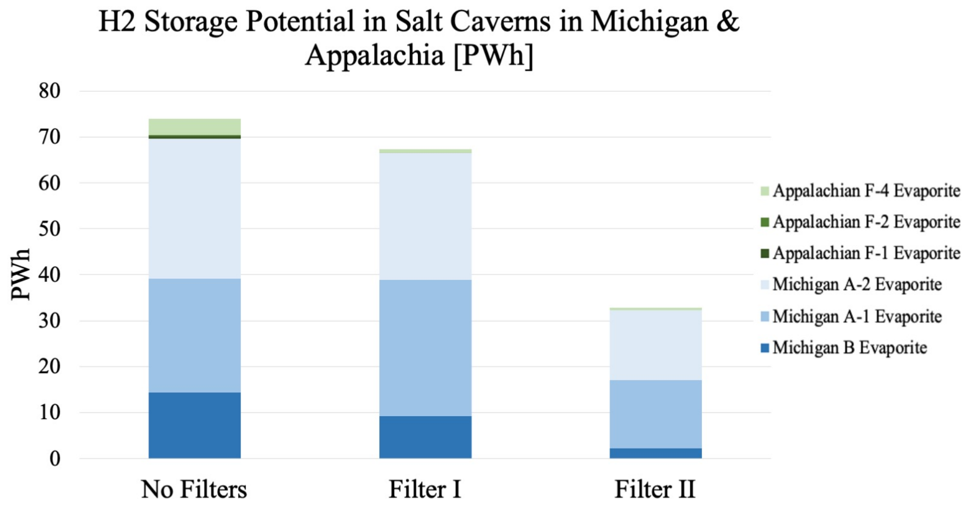

Figure 7. Bar chart showing hydrogen storage potential [PWh] in the evaporite layers across the Michigan (blue gradient) and Appalachian (green gradient) regions. Filter scenarios highlight higher value caverns. Filter I only considers grid cell with less than 7 caverns. Filter II includes Filter I while also excluding caverns that require more cushion gas than their working gas capacity.

Table 2 shows the cumulative hydrogen storage potential across the overlaid analyzed layers in Michigan and Appalachia. Figure 7 is the bar chart that visualizes these results. We can see here that the working gas potential in Michigan is 2.1×10^9 metric tons of H_2, or 69.9 PWh, while in Appalachia it is $1.32{\times}10^8$ metric tons of H_2, or 4.4 PWh. It is likely, however, that not all of these resources will be developed and that instead, we will focus on the higher value caverns. While this paper does not focus on the techno-economics of cavern construction, we can utilize two heuristics to broadly infer higher value regions. From Papadias and Ahluwalia (2021), the two conditions that are likely to drive up cost are :

1. Installation costs for building multiple caverns instead of fewer larger caverns, taking into consideration constraints from the existence of impure interlayers.
   From this heuristic we can infer that grid cells that have thicker salts and therefore fewer numbers of caverns built are more valuable. With this criterion, we apply Filter I, which removes all the grid cells that have more than 7 caverns, leaving us with Michigan at 66.5 PWh, while in Appalachia it is 0.85 PWh of H_2 working gas potential in salt caverns.
2. A high cushion gas requirement given the high cost of producing hydrogen.
   From this heuristic we can infer that caverns with a high ratio of working gas to cushion gas are desirable. Therefore, in Filter II we add onto the constraints of Filter I and remove all the caverns that have more cushion gas than working gas. This results in Michigan having 32.36 PWh, while in Appalachia the working gas potential is reduced to 0.54 PWh. While these filters cut the total working gas potential roughly in half and significantly reduce the potential of the Appalachian region, they are noticeably still within quite large. As a reminder, the current total underground natural gas storage capacity is 1.37 PWh, meaning that, disre-

Table 2. Hydrogen storage capacity with different filtering scenarios. 1 PWh = 1000 TWh. Filter 1 and 2 represent subsets of storage potential that meet specific technical criteria that would favor commercial deployment: a) Filter 1 consider those grid cells with 7 or lower caverns, since additional caverns add investment costs, b) Filter 2 considers the Filter 1 criteria and removes all caverns where cushion gas mass exceeds working gas mass. All numbers reported on a lower heating value (LHV) basis.

[PWh]	No Filters	Filter I	Filter II
Total Capacity	80.9	67.4	32.9
Michigan B Evaporite	30.4	27.6	15.3
Michigan A-1 Evaporite	14.3	9.31	2.2
Michigan A-2 Evaporite	24.9	29.6	14.8
Appalachian F-1 Evaporite	0.53	0.05	0.00
Appalachian F-2 Evaporite	0.27	0.00	0.00
Appalachian F-4 Evaporite	3.6	0.81	0.54

garding the important spatial placement and hydrogen transportation needs, these regions alone could physically meet our underground energy storage needs.

In Figure 7, we can also appreciate differences in the salt resource potential. The Michigan Evaporites clearly dominate the total potential working gas capacity across both regions, with the Michigan A-2 Evaporite representing the greater share of potential within Michigan. In Appalachia, the F-4 Evaporite clearly dominates this region's working gas capacity potential and even after the application of the filters offers a storage capacity of 0.540 PWh.

4 Key Findings

In this paper, we have presented a new approach to assess resource potential for hydrogen storage in salt caverns, based on physical well-log interpretations and a physical model grounded in geomechanical considerations. Our approach captures and considers the heterogeneity of geological hydrogen storage, constrained by both above-ground safety and below-ground physical considerations. Our main contributions are:

1. A new geologic interpretation of the Salina Group in the Michigan Basin and Appalachian salt basins considered for hydrogen storage in salt caverns.
2. A simple analytical geomechanical model that calculates the cavern's hydrogen storage potential under a variety of scenarios.
3. A spatial resource analysis that includes excluded areas due to safety or environmental concerns. Our analysis shows that the total technical working gas potential in Michigan is 2.1×10^9 metric tons of H_2 or 69.9 PWh while in Appalachia it is 1.3×10^8 metric tons of H_2 or 4.4 PWh. .

Our geophysical model (Section 2.2.5) shows that there exists an optimal depth range for cavern construction that, based on the Salina rheological parameters, occurs within the approximate range of 1000 m to 1700 m, with the optimal depth at 1500 m. This finding clarifies the heuristics presented in the literature and allows for estimations and visualizations of the physical potential of hydrogen storage to a new degree of accuracy.

Our capacity analysis (Section 3.3) shows that the overall technical working gas potential in Michigan is 2.1×10^9 metric tons of H_2, or 69.9 PWh, while in Appalachia, it is 1.32×10^8 metric tons of H_2, or 4.4 PWh. After applying the two above-mentioned filters, these potentials are reduced to 32.4 PWh in the case of Michigan and 0.54 PWh in Appalachia. These are significant quantities, especially when compared to the US' current underground NG working gas capacity of 1.375 PWh. For a single 500 × 500 m^2 area, the maximum total storable H_2 working gas potential reaches 380 GWh, or 11 400 metric ton, with an energy density of 398 $\mathrm{kW\,h\,m^{-3}}$.

When comparing the physical potential of the studied regions, Michigan has purer and more abundant salts than Appalachia. This advantage translates to approximately 15 times the hydrogen working gas storage capacity for cases with minimal constraints and approximately 60 times with more restrictive constraints when compared to Appalachia. Furthermore, the formation of the Appalachian Mountains likely resulted in the deformation of the Appalachian basin fill, potentially causing notable variations in our salt layer thickness estimations which may distort our results for the region. Overall, our research represents an advance in the understanding of hydrogen storage in salt caverns, particularly within the context of the United States, and provides a solid foundation for future work in this field.

5 Future Work

In this paper, we quantify the availability of hydrogen storage resources in salt caverns in Michigan and the Appalachian region. This analysis emphasizes the physical capacity of storage; however, it is equally important to understand the techno-economics of storage when compared to other potential hydrogen storage methods. Future work could look into understanding the techno-economic outlook for H_2 storage development in these regions considering their role in balancing supply and demand in future low-carbon energy systems. Such an analysis could be undertaken by representing the technical and economic attributes of these resources in the multi-sector energy system planning models to study how their availability impacts overall energy system in terms of system cost and infrastructure deployment under various technology and policy scenarios.

In addition, our approach and in-depth analysis could be expanded to other salt basins in North America to better understand and compare these resources. The basins that we suggest targeting in the US are the Permian basin, the Gulf Coast basin, the Williston basin, the Sevier Valley basin, and the Paradox basin.

Appendix A Minimum Pressure by Creep

Salt ductile failure is highly dependent on the deviatoric strain rate $\dot{\varepsilon}$ which is highly sensitive to the deviatoric shear stress σ, and less so to the temperature T and the activation energy Q:

$$\dot{\varepsilon} = A \exp\left(\frac{-Q}{RT}\right) \sigma^n \tag{A1}$$

Where the gas constant $R = 8.3144\,\mathrm{m^3\,Pa\,K^{-1}\,mol^{-1}}$. Because the strain rate depends on the shear stress raised to the power n, this is called power law flow. In the salt context, it is often referred to as the Norton flow law.

The three parameters A, Q, and n are determined experimentally by measuring $\dot{\varepsilon}$ at multiple values of σ and T and performing a fitting exercise to constrain the parameters. This is experimentally challenging and there are considerable uncertainties in estimates of individual parameters, as well as substantial covariance among estimates (Berest & Brouard, 1998; L. Ma et al., 2021; Nye & Mott, 1953).

The covariance between A and n makes comparing estimates of flow parameters from different studies difficult. In particular, the dimensions of the parameter A are MPa^{-n}, so the units of A depend on the stress exponent. This complication can be removed by a change in variable: $A^* = \frac{A}{(\sigma^*)^n}$, where σ^* is a reference stress. If $\sigma^* = 1\,\mathrm{MPa}$, then

$A^* = A$. Alternatively, as we discuss later, the reference stress σ^* can be chosen to obtain a particular value of A^*.

It is also useful to define the parameter $T^* = \frac{Q}{R}$ such that the thermal activation term in (A1) becomes $e^{\left(\frac{-T^*}{T}\right)}$. The effects of temperature variations depend on how large these temperature variations are compared to T^*. If we ignore the effects of temperature variations, it is useful to define a reference temperature, T_{ref}, and rewrite (A1) as

$$\dot{\varepsilon} = D^* \left(\frac{\sigma}{\sigma^*}\right)^n = A^* \exp\left(\frac{-T^*}{T_{\text{ref}}}\right)\left(\frac{\sigma}{\sigma^*}\right)^n \tag{A2}$$

There are analytic expressions for the ductile collapse of spherical and cylindrical voids in a whole space consisting of a power law fluid (X. Ma et al., 2021). The radial inflow velocity at the cavern wall is easily related to the volumetric collapse rate. The contraction rates for a sphere and a cylinder are very similar, differing only by a constant term. The rate at which the cavern collapses is proportional to its volume, leading to an exponential decrease in cavern volume with time. The rate at which the volume changes, which depends on the difference between the far-field lithostatic stress, p_{lith}, and the cushion gas pressure, p_{c}, is given by:

$$\frac{d\ln V}{dt} = \frac{\dot{V}}{V} = -\alpha^{(n+1)} n^{-n} D^* \left[\frac{(p_{\text{lith}} - p_{\text{c}})}{\sigma^*}\right]^n \tag{A3}$$

Here $\alpha = \frac{3}{2}$ for a sphere and $\alpha = \sqrt{3}$ for a cylinder.

Equation (A3) can be integrated to calculate the volume of the cavern as a function of time:

$$V = V_0 \exp\left(-\alpha^{(n+1)} n^{-n} D^* \left[\frac{(p_{\text{lith}} - p_{\text{c}})}{\sigma^*}\right]^n t\right) \tag{A4}$$

Here V_0 is the initial cavern volume. We assume that a collapse rate of 30% over 30 years as an acceptable loss of volume over time (X. Ma et al., 2021). Integrating (A4) for 30 years, a 30% decrease in volume would result for

$$D'^* = \alpha^{(n+1)} n^{-n} D^* \left[\frac{(p_{\text{lith}} - p_{\text{c}})}{\sigma^*}\right]^n = \frac{0.012}{\text{year}}, \tag{A5}$$

for $\sigma^* = p_{\text{lith}} - p_{\text{c}}$.

Then, solving for the critical stress σ^*,

$$\sigma^* = \left[\frac{1}{n}\left(\frac{0.012}{D'^* \alpha^{(n+1)}}\right)\right]^{1/n} \tag{A6}$$

Here, σ^* represents a critical stress difference where the contraction rate changes from being negligible to large fairly rapidly. When $\left[\frac{(p_{\text{lith}} - p_{\text{c}})}{\sigma^*}\right]$ is less than one, raising it to the power n gives a small contraction rate. When $\left[\frac{(p_{\text{lith}} - p_{\text{c}})}{\sigma^*}\right]$ is greater than one, raising it to the power n gives a large contraction rate.

There is a wide range in estimates of the rheological parameters describing power law creep of salt. In addition, the temperature of candidate reservoirs varies. Thus, the value of the critical stress σ^* for a particular candidate reservoir must be determined via a special study. After an extensive literature review (Berest & Brouard, 1998; H. Li et al., 2021; X. Ma et al., 2021; Michael Susan, 2019; Wawersik & Zeuch, 1986), we collected 19 sets of rheological parameters from across the world which are compiled in Table A1.

Table A1. Compilation of rheological parameters for salts. First 15 facilities were collected by Berest and Brouard (1998) while the rest were collected by the author named in the Facility column. The last columns refer σ^* values calculated at different reference temperatures of 310 K and 340 K respectively.

No.	Facility	n	T^* [K]	A [MPa^{-n}/year]	σ^*_{310} (MPa)	σ^*_{340} (MPa)
1	Avery Island (after D.V.)	3.14	6495	1.30×10^4	14.4	8.0
2	WIPP	5.00	5035	1.04	27.3	20.5
3	Salado (WIPP7)	5.09	8333	3.67×10^4	27.6	17.3
4	Asse (after W.)	6.25	9969	2.51×10^4	55.3	35.1
5	West Hackberry (WH1)	4.73	6606	4.52×10^2	23.7	15.9
6	West Hackberry (WH2)	4.99	10 766	9.40×10^{-1}	1134.4	613.8
7	Bryan Mound (BM3C)	4.54	7623	1.32×10^3	40.5	25.1
8	Bryan Mound (BM4C)	5.18	8977	1.04	304.4	185.9
9	Bayou Choctaw (BC I)	4.06	5956	6.40×10^1	28.1	18.5
10	Etrez	3.10	4100	6.40×10^{-1}	29.6	20.3
11	Avery Island (after S. and al.)	4.00	6565	2.08×10^3	19.7	12.3
12	Salina	4.10	8715	2.78×10^5	31.5	17.2
13	Palo Duro - Unit 4	5.60	9760	1.81×10^5	42.4	25.8
14	Palo Duro - Unit 5	5.30	9810	2.52×10^5	44.9	26.5
15	Asse (B.G.R.)	5.00	6495	6.57×10^1	30.5	21.1
16	X. Ma et al. (2021)	3.50	0	6.00×10^{-6}	15.2	15.2
17	Michael Susan (2019)	5.00	6495	1.32×10^2	26.6	18.3
18	Wawersik and Zeuch (1986)	5.00	6485	2.29×10^2	23.6	16.3
19	J. Li et al. (2020)	3.50	0	1.50×10^{-6}	22.5	22.5

From this table, we utilize the measure Ohio Salina rheological parameters (Berest & Brouard, 1998):

$$n = 4.1,$$
$$T^* = 8715\,\mathrm{K},$$
$$A^* = 2.7752 \times 10^5\,\mathrm{MPa}^{-n}.$$

These values were chosen because the Salina evaporite formation is shared across Michigan, Ohio, and the Appalachian region and we infer can serve as a good approximation to the rheological properties of the studied regions.

If instead, we use the median values from this table, Figure A1 highlights resulting pressure differentials as a function of depth, similar to the plot noted for the Salina salts Figure 3. By comparing both of these plots, we can see that the rheological parameters impact the optimum depth where in the case of the Ohio Salina rheological values seen in Figure 3, the optimum depth is approximately 1500 m while the optimum depth for the median rheological values is approximately 1250 m.

Appendix B Note On Horizontal Cylindrical Cavern Shapes

Horizontal caverns can be thought of as a series of spherical caverns that overlap on the same horizontal line. These shapes are attractive since they would allow for larger volumetric caverns within the same bedded salt which would allow for savings in installation equipment and operating costs. Innovations in horizontal drilling technologies in the 90s led to a surge in interest and studies in the possibility of utilizing the horizontal cavern shape. These studies concluded that although the structure of the caverns are stable, the construction process is difficult, lengthy, and therefore expensive (Kunstman

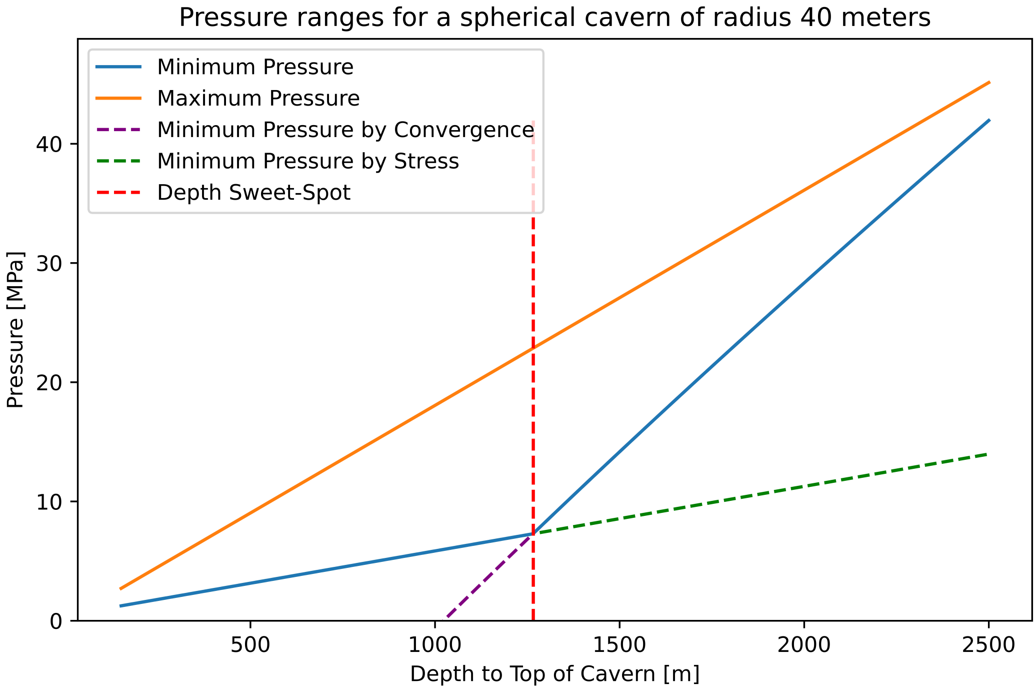

Figure A1. Pressure ranges for a spherical cavern of radius 40 meters when taking the median rheological parameters from Table A1. The depth "sweet spot," slightly deeper than $D = 1250\,\text{m}$, can be approximated as the pressure where the minimum pressure ductile failure (Eqs difference Δp_{max} (7)) overcomes the brittle failure (Eq (5)) leading to the largest working gas pressure difference Δp_{max}. If creep were ignored, Δp would increase with depth as seen by the widening difference between the Maximum Pressure orange line and the Minimum Pressure by stress dashed green line.

& Urbanczyk, Kazimierz M., 1995; Thoms & Gehle, 1993). However, given the growing interest in hydrogen storage—a gas that demands larger storage volumes of storage compared to natural gas (Wallace et al., 2021)—and a scarcity of thick bedded salt deposits globally, there is a renewed interest in further understanding and evaluating the viability of horizontally oriented cylindrical caverns, particularly in the context of China (Liu et al., 2019, 2020; Wan et al., 2019; Ban et al., 2021).

Overall, the storage potential calculations are similar to that of the spherical cavern with the main difference given by the potential cavern volume being much larger for horizontal cylinders where the volume of a cylindrical cavern is given by:

$$V_{\text{cylinder}} = \pi r^2 L \tag{B1}$$

Where we take L, the length of the cylinder, to be as long as desired or as allowed by the salt formations.

Acronyms

VRE Variable Renewable Energy
H_2 Hydrogen Molecule
IEA International Energy Agency

NG Natural Gas
SPR Strategic Petroleum Reserve
ESOGIS Empire State Organized Geologic Information System
ASH Appalachian Storage Hub
EDWIN Exploration and Development Wells Information Networ
DEM Digital Elevation Map
IOGCC Interstate Oil and Gas Compact Commission
GLAES Geospatial Land Availability for Energy System
USGS United State Geological Survey

Appendix C Open Research

The physical well logs that were used are proprietary and we were not granted permission to share them.

The Michigan basin physical well logs were provided by the Dr. William Harrison and Dr. Peter J. Voice from the Michigan Geological Repository for Research and Education at Western Michigan University. These physical well logs may be accessed by reaching out and requesting the data to these the mentioned researchers.

The Appalachian basin physical well logs were data-mined from publicly available geophysical databases at the state-level. While we do not have permission to share these files directly, other researchers may gain access through the following file repositories:

- The Empire State Organized Geologic Information System (ESOGIS) from New York State.
- The Appalachian Basin Tight Gas Reservoirs Project File Repository provided by the Appalachian Oil and Natural Gas Research Consortium for West Virginia and Pennsylvania.
- The "Pipeline" oil and gas well data repository through the West Virginia Geological and Economic Survey.
- The West Virginia Geological and Economic Survey digitized logs file server.
- The Appalachian Storage Hub (ASH) Project File and Data Search contains well files from Ohio, West Virginia, and Pennsylvania.
- The Exploration and Development Wells Information Network (EDWIN) from Pennsylvania.

We can, however, share the resulting salt maps, exclusion zones, and Python scripts that were utilized in the analysis. The salt basin data and Python scripts used for the mapping and analysis in the study are available at the Mendley Data repository via: `https://data.mendeley.com/datasets/rrn4x86x7y/1`

Acknowledgments

We thank Dr. William Harrison and Dr. Peter J. Voice from the Michigan Geological Repository for Research and Education at Western Michigan University for sharing their database of geophysical well logs from the Michigan Basin with us as well as their knowledge and expertise on the evaporites in the region. Funding for this project was provided by Shell Global Solutions International.

References

Abreu, J. F., Costa, A. M., Costa, P. V., Miranda, A. C., Zheng, Z., Wang, P., ... Nishimoto, K. (2023). Large-scale storage of hydrogen in salt caverns for carbon footprint reduction. *International Journal of Hydrogen Energy*, *48*, 14348–14362. Retrieved from `https://www.sciencedirect.com/science/article/pii/S0360319922061298` doi: 10.1016/j.ijhydene.2022.12.272

Albertus, P., Manser, J. S., & Litzelman, S. (2020, January). Long-Duration Electricity Storage Applications, Economics, and Technologies. *Joule*, *4*(1), 21–32. Retrieved 2023-10-20, from `https://www.cell.com/joule/abstract/S2542-4351(19)30539-2` (Publisher: Elsevier) doi: 10.1016/j.joule.2019.11.009

Alessandra Simone, Anna Morisani-Zechmeister, & Frank Frey. (2021, September). *Preparing for a Hydrogen Future – Constraints and Alternatives for Hydrogen Storage* (Tech. Rep.). GHD, Houston, TX, USA: Salt Mining Institute.

Allen, R. D., Doherty, T. J., & Thoms, R. L. (1982, May). *Geotechnical factors and guidelines for storage of compressed air in solution-mined salt cavities* (Tech. Rep. No. PNL-4242). Pacific Northwest Lab., Richland, WA (USA). Retrieved 2022-01-06, from `https://www.osti.gov/biblio/5234728` doi: 10.2172/5234728

Atkins. (2018). *Hydrogen turbines follow on - salt cavern appraisal for hydrogen and gas storage - appendices* (Tech. Rep.). UK Energy Research Centre Energy Data Centre (UKERC EDC). Retrieved from `https://ukerc.rl.ac.uk/cgi-bin/eti_query.pl?GoButton=DisplayLanding&etiID=271` (Accessed: 2022-09-20. Medium: pdf. Publisher: ETI) doi: 10.5286/UKERC.EDC.000133

Ban, F., Yuan, G., Wan, J., & Peng, T. (2021, December). The optimum interwell distance analysis of two-well-horizontal salt cavern construction. *Energy Sources, Part A: Recovery, Utilization, and Environmental Effects*, *43*(23), 3082–3100. Retrieved 2022-01-01, from `https://doi.org/10.1080/15567036.2020.1851323` (Publisher: Taylor & Francis _eprint: https://doi.org/10.1080/15567036.2020.1851323) doi: 10.1080/15567036.2020.1851323

Bell, I. H., Wronski, J., Quoilin, S., & Lemort, V. (2014, February). Pure and Pseudo-pure Fluid Thermophysical Property Evaluation and the Open-Source Thermophysical Property Library CoolProp. *Industrial & Engineering Chemistry Research*, *53*(6), 2498–2508. Retrieved 2023-10-30, from `https://doi.org/10.1021/ie4033999` (Publisher: American Chemical Society) doi: 10.1021/ie4033999

Berest, P., & Brouard, B. (1998, April 19-22). *A tentative classification of salts according to their creep properties* (Tech. Rep.). New Orleans, Louisiana, USA: Solution Mining Research Institute (SMRI). (Available online at https:https://biblio.brouard-consulting.com/smri-new-orleans-98.pdf)

Bérest, P., & Brouard, B. (2003). Safety of salt caverns used for underground storage blow out; mechanical instability; seepage; cavern abandonment. *Oil & Gas Science and Technology - Revue d'IFP Energies nouvelles*, *58*(3), 361–384. Retrieved from `https://ogst.ifpenergiesnouvelles.fr/articles/ogst/abs/2003/03/berest_58n3/berest_58n3.html` doi: 10.2516/ogst:2003023

Bødal, E. F., Mallapragada, D., Botterud, A., & Korpås, M. (2020, November). Decarbonization synergies from joint planning of electricity and hydrogen production: A Texas case study. *International Journal of Hydrogen Energy*, *45*(58), 32899–32915. Retrieved 2021-10-05, from `https://www.sciencedirect.com/science/article/pii/S0360319920335679` doi: 10.1016/j.ijhydene.2020.09.127

Caglayan, D. G., Weber, N., Heinrichs, H. U., Linßen, J., Robinius, M., Kukla, P. A., & Stolten, D. (2020, February). Technical potential of salt caverns for hydrogen storage in Europe. *International Journal of Hydrogen Energy*, *45*(11), 6793–6805. Retrieved 2021-10-06, from `https://linkinghub.elsevier.com/retrieve/pii/S0360319919347299` doi: 10.1016/j.ijhydene.2019.12.161

Crotogino, F. (2016). Larger scale hydrogen storage. In T. M. Letcher

(Ed.), *Storing energy: With special reference to renewable energy sources* (p. 411-430). Elsevier. Retrieved from http://dx.doi.org/10.1016/B978-0-12-803440-8.00020-8 doi: 10.1016/B978-0-12-803440-8.00020-8

Crotogino, F. (2022, January). 26 - Large-scale hydrogen storage. In T. M. Letcher (Ed.), *Storing Energy (Second Edition)* (pp. 613–632). Elsevier. Retrieved 2023-03-01, from https://www.sciencedirect.com/science/article/pii/B9780128245101000039 doi: 10.1016/B978-0-12-824510-1.00003-9

Denholm, P., Cole, W., & Blair, N. (2023, September). *Moving beyond 4-hour li-ion batteries: Challenges and opportunities for long(er)-duration energy storage* (Technical Report No. NREL/TP-6A40-85878). Golden, CO: National Renewable Energy Laboratory. Retrieved from https://www.nrel.gov/docs/fy23osti/85878.pdf

Dinescu, S., Radu, S. M., Florea, A., Danciu, C., Tomuș, O. B., & Popescu, S. (2021). Possible risks of co2 storage in underground salt caverns. *Annals of the University of Petroșani, Mechanical Engineering*, *23*, 27-36. Retrieved from https://www.upet.ro/annals/mechanical/pdf/2021/04_Dinescu_et_al.pdf

Dopffel, N., Mayers, K., Kedir, A., Alagic, E., An-Stepec, B. A., Djurhuus, K., ... Hoth, S. (2023, June). Microbial hydrogen consumption leads to a significant pH increase under high-saline-conditions: implications for hydrogen storage in salt caverns. *Scientific Reports*, *13*(1), 10564. Retrieved 2023-07-04, from https://www.nature.com/articles/s41598-023-37630-y (Number: 1 Publisher: Nature Publishing Group) doi: 10.1038/s41598-023-37630-y

Duffy, O., Moscardelli, L., Hudec, M., & Shuster, M. (2021, October). Assessing the hydrogen storage potential of onshore texas salt structures. In *Gulf coast association of geological societies 2021 annual meeting.* Austin, Texas. (Presentation at the Gulf Coast Association of Geological Societies 2021 Annual Meeting, Austin, Texas)

Energy Resource Committee of the Interstate Oil and Gas Compact Commission (IOGCC). (1995). *Natural gas storage in salt caverns: A guide for design and construction* (Tech. Rep.). Oklahoma City, OK: Interstate Oil and Gas Compact Commission. (Available online: URL-where-document-can-be-accessed,)

Fabig, T., & Brückner, D. (2011). *Case studies for cyclic operated storage caverns 'aardgasbuffer zuidwending' nl* (Tech. Rep. No. B IfG 49/2011). Leipzig, Germany: IfG.

Harrison, W., Voice, P., & Caruthers, A. (2016, January). Salina group lithofacies in the michigan basin: A review from A to G.. doi: 10.1130/abs/2016NC-275296

Horváth, P. L., Mirau, S., Schneider, G.-S., Bernhardt, H., Weiler, C., Bödeker, J., ... Ratigan, J. (2018). *Update of smri's compilation of worldwide salt deposits and salt cavern fields* (Tech. Rep.). Available online: https://www.researchgate.net/publication/348603174_Update_of_SMRIs_Compilation_of_Worldwide_Salt_Deposits_and_Salt_Cavern_Fields: Solution Mining Research Institute (SMRI).

International Energy Agency. (2021). *Net zero by 2050.* https://www.iea.org/reports/net-zero-by-2050. Paris. (License: CC BY 4.0)

Jenkins, J. D., & Sepulveda, N. A. (2021, September). Long-duration energy storage: A blueprint for research and innovation. *Joule*, *5*(9), 2241–2246. Retrieved 2023-10-20, from https://linkinghub.elsevier.com/retrieve/pii/S2542435121003585 doi: 10.1016/j.joule.2021.08.002

Kunstman, A. S., & Urbanczyk, Kazimierz M. (1995). Modelling of horizontal cavern leaching: main aspects and perspectives. *Solution Mining Research Institute (SMRI).*

Lackey, G., Freeman, G. M., Buscheck, T. A., Haeri, F., White, J. A., Huerta, N., & Goodman, A. (2023). Characterizing Hydrogen Storage Potential in U.S. Underground Gas Storage Facilities. *Geophysical Research Letters*, *50*(3), e2022GL101420. Retrieved 2023-10-31, from https://onlinelibrary.wiley.com/doi/abs/10.1029/2022GL101420 (_eprint: https://onlinelibrary.wiley.com/doi/pdf/10.1029/2022GL101420) doi: 10.1029/2022GL101420

Lankof, L., & Tarkowski, R. (2020, July). Assessment of the potential for underground hydrogen storage in bedded salt formation. *International Journal of Hydrogen Energy*, *45*(38), 19479–19492. Retrieved 2022-02-09, from https://linkinghub.elsevier.com/retrieve/pii/S0360319920317523 doi: 10.1016/j.ijhydene.2020.05.024

Lankof, L., Urbańczyk, K., & Tarkowski, R. (2022, February). Assessment of the potential for underground hydrogen storage in salt domes. *Renewable and Sustainable Energy Reviews*, *160*, 112309. doi: 10.1016/j.rser.2022.112309

Leachman, J. W., Jacobson, B., Penoncello, S., & Lemmon, E. (2009, September). Fundamental Equations of State for Parahydrogen, Normal Hydrogen, and Orthohydrogen. *NIST*, *38*(3), 721–748. Retrieved 2023-10-30, from https://www.nist.gov/publications/fundamental-equations-state-parahydrogen-normal-hydrogen-and-orthohydrogen (Last Modified: 2021-10-12T11:10-04:00 Publisher: Jacob W. Leachman, Bryce Jacobson, Steven Penoncello, Eric Lemmon)

Li, H., Deng, J., Wanyan, Q., Feng, Y., Kamgue Lenwoue, A. R., Luo, C., & Hui, C. (2021, May). Numerical Investigation on Shape Optimization of Small-Spacing Twin-Well for Salt Cavern Gas Storage in Ultra-Deep Formation. *Energies*, *14*(10), 2859. Retrieved 2023-12-27, from https://www.mdpi.com/1996-1073/14/10/2859 doi: 10.3390/en14102859

Li, J., Yang, C., Shi, X., Xu, W., Li, Y., & Daemen, J. J. K. (2020, July). Construction modeling and shape prediction of horizontal salt caverns for gas/oil storage in bedded salt. *Journal of Petroleum Science and Engineering*, *190*, 107058. Retrieved 2022-02-23, from https://www.sciencedirect.com/science/article/pii/S0920410520301510 doi: 10.1016/j.petrol.2020.107058

Liu, W., Zhang, Z., Chen, J., Fan, J., Jiang, D., Jjk, D., & Li, Y. (2019, October). Physical simulation of construction and control of two butted-well horizontal cavern energy storage using large molded rock salt specimens. *Energy*, *185*, 682–694. Retrieved 2022-11-30, from https://www.sciencedirect.com/science/article/pii/S0360544219313416 doi: 10.1016/j.energy.2019.07.014

Liu, W., Zhang, Z., Chen, J., Jiang, D., Wu, F., Fan, J., & Li, Y. (2020, May). Feasibility evaluation of large-scale underground hydrogen storage in bedded salt rocks of China: A case study in Jiangsu province. *Energy*, *198*, 117348. Retrieved 2021-10-28, from https://www.sciencedirect.com/science/article/pii/S0360544220304552 doi: 10.1016/j.energy.2020.117348

Lord, A. S., Kobos, P. H., & Borns, D. J. (2014, September). Geologic storage of hydrogen: Scaling up to meet city transportation demands. *International Journal of Hydrogen Energy*, *39*(28), 15570–15582. Retrieved 2021-10-05, from https://www.sciencedirect.com/science/article/pii/S0360319914021223 doi: 10.1016/j.ijhydene.2014.07.121

Lux, K.-H. (2009, 01). Design of salt caverns for the storage of natural gas, crude oil and compressed air: Geomechanical aspects of construction, operation and abandonment. In *Underground Gas Storage: Worldwide Experiences and Future Development in the UK and Europe.* Geological Society of London. Retrieved from https://doi.org/10.1144/SP313.7 doi: 10.1144/SP313.7

Ma, L., Wang, Y., Wang, M., Xue, B., & Duan, L. (2021, May). Mechanical properties of rock salt under combined creep and fatigue. *International Journal of Rock Mechanics and Mining Sciences*, *141*, 104654. Retrieved 2022-04-06, from https://linkinghub.elsevier.com/retrieve/pii/S1365160921000411 doi: 10.1016/j.ijrmms.2021.104654

Ma, X., Xu, Z., Chen, L., & Shi, X. (2021, March). Creep deformation analysis of gas storage in salt caverns. *International Journal of Rock Mechanics and Mining Sciences*, *139*, 104635. Retrieved 2022-03-13, from https://www.sciencedirect.com/science/article/pii/S136516092100023X doi: 10.1016/j.ijrmms.2021.104635

Matos, C. R., Carneiro, J. F., & Silva, P. P. (2019, February). Overview of Large-Scale Underground Energy Storage Technologies for Integration of Renewable Energies and Criteria for Reservoir Identification. *Journal of Energy Storage*, *21*, 241–258. Retrieved 2023-12-26, from https://www.sciencedirect.com/science/article/pii/S2352152X18301919 doi: 10.1016/j.est.2018.11.023

Michael Susan. (2019). *Exploring the Energy Storage Capacity of Salt Caverns in the Netherlands.*

Michigan Department of Environment, Great Lakes, and Energy. (2024). *Injection wells in michigan.* Retrieved from https://www.michigan.gov/egle/about/organization/oil-gas-and-minerals/oil-and-gas/injection-wells-in-michigan (Accessed: 2024-02-26)

Nye, J. F., & Mott, N. F. (1953, October). The flow law of ice from measurements in glacier tunnels, laboratory experiments and the Jungfraufirn borehole experiment. *Proceedings of the Royal Society of London. Series A. Mathematical and Physical Sciences*, *219*(1139), 477–489. Retrieved 2022-03-04, from https://royalsocietypublishing.org/doi/10.1098/rspa.1953.0161 (Publisher: Royal Society) doi: 10.1098/rspa.1953.0161

Ocko, I. B., & Hamburg, S. P. (2022, July). Climate consequences of hydrogen emissions. *Atmospheric Chemistry and Physics*, *22*(14), 9349–9368. Retrieved 2022-11-15, from https://acp.copernicus.org/articles/22/9349/2022/ doi: 10.5194/acp-22-9349-2022

Ozarslan, A. (2012, October). Large-scale hydrogen energy storage in salt caverns. *International Journal of Hydrogen Energy*, *37*(19), 14265–14277. Retrieved 2021-10-05, from https://www.sciencedirect.com/science/article/pii/S0360319912017417 doi: 10.1016/j.ijhydene.2012.07.111

Panfilov, M. (2016, December). Underground and pipeline hydrogen storage. In (pp. 91–115). doi: 10.1016/B978-1-78242-362-1.00004-3

Papadias, D. D., & Ahluwalia, R. K. (2021, October). Bulk storage of hydrogen. *International Journal of Hydrogen Energy*, *46*(70), 34527–34541. Retrieved 2022-09-09, from https://www.sciencedirect.com/science/article/pii/S0360319921030834 doi: 10.1016/j.ijhydene.2021.08.028

Parkes, D., Evans, D., Williamson, P., & Williams, J. (2018, August). Estimating available salt volume for potential CAES development: A case study using the Northwich Halite of the Cheshire Basin. *Journal of Energy Storage*, *18*, 50–61. Retrieved 2022-01-20, from https://linkinghub.elsevier.com/retrieve/pii/S2352152X18301233 doi: 10.1016/j.est.2018.04.019

Rand, J., Bolinger, M., Wiser, R., Jeong, S., & Paulos, B. (2021, May). *Queued Up: Characteristics of Power Plants Seeking Transmission Interconnection As of the End of 2022* (Tech. Rep. Nos. None, 1784303, ark:/13030/qt5jd5x0q9). Retrieved 2023-10-20, from https://www.osti.gov/servlets/purl/1784303/ doi: 10.2172/1784303

Ryberg, D. S., Robinius, M., & Stolten, D. (2017, December). *Methodological Framework for Determining the Land Eligibility of Renewable Energy Sources* (Tech. Rep. No. arXiv:1712.07840). arXiv. Retrieved 2022-06-07, from http://arxiv.org/abs/1712.07840 (arXiv:1712.07840 [cs] type: article) doi: 10.48550/arXiv.1712.07840

Sainz-Garcia, A., Abarca, E., Rubi, V., & Grandia, F. (2017, June). Assessment of feasible strategies for seasonal underground hydrogen storage in a saline aquifer. *International Journal of Hydrogen Energy*, *42*(26), 16657–16666. Retrieved 2023-12-26, from https://www.sciencedirect.com/science/article/pii/S0360319917319420 doi: 10.1016/j.ijhydene.2017.05.076

Schuba, C. N., & Moscardelli, L. (2023). Subsurface storage in the mississippi salt basin domes: Considerations for the emerging hydrogen economy. *AAPG Bulletin*, *107*(11), 1957–1970. doi: 10.1306/05302322160

Sepulveda, N. A., Jenkins, J. D., Edington, A., Mallapragada, D. S., & Lester, R. K. (2021, March). The design space for long-duration energy storage in decarbonized power systems. *Nature Energy*, *6*(5), 506–516. Retrieved 2023-10-20, from https://www.nature.com/articles/s41560-021-00796-8 doi: 10.1038/s41560-021-00796-8

Stone, H., Veldhuis, I., & Richardson, R. (2009, May). Underground hydrogen storage in the UK. *Geological Society of London Special Publications*, *313*, 217–226. doi: 10.1144/SP313.13

Tarkowski, R., Uliasz-Misiak, B., & Tarkowski, P. (2021, June). Storage of hydrogen, natural gas, and carbon dioxide – Geological and legal conditions. *International Journal of Hydrogen Energy*, *46*(38), 20010–20022. Retrieved 2021-10-06, from https://linkinghub.elsevier.com/retrieve/pii/S0360319921010454 doi: 10.1016/j.ijhydene.2021.03.131

Thoms, R., & Gehle, R. (1993, October 24-27). Feasibility of controlled solution mining from horizontal wells. In *Proceedings of the 1993 fall meeting, solution mining research institute (smri).* Lafayette, Louisiana, USA. (Presented at the 1993 Fall Meeting in Lafayette, Louisiana)

U.S. Energy Information Administration (EIA). (2024). *Underground natural gas working storage capacity.* https://www.eia.gov/dnav/ng/ng_stor_cap_dcu_nus_a.htm. (Accessed on [insert date here])

Voice, P., Harrison, W., & Caruthers, A. (2017). *Salina Group Lithofacies in the Michigan Basin: Development of an Improved Depositional Model From Core Analysis.*

Wallace, R. L., Cai, Z., Zhang, H., Zhang, K., & Guo, C. (2021, July). Utility-scale subsurface hydrogen storage: UK perspectives and technology. *International Journal of Hydrogen Energy*, *46*(49), 25137–25159. Retrieved 2021-10-20, from https://www.sciencedirect.com/science/article/pii/S0360319921017481 doi: 10.1016/j.ijhydene.2021.05.034

Wan, J., Peng, T., Shen, R., & Jurado, M. J. (2019, August). Numerical model and program development of TWH salt cavern construction for UGS. *Journal of Petroleum Science and Engineering*, *179*, 930–940. Retrieved 2023-12-31, from https://www.sciencedirect.com/science/article/pii/S092041051930364X doi: 10.1016/j.petrol.2019.04.028

Wang, T., Li, J., Zhang, Q., Yang, C., & Daemen, J. (2019, January). Determination of the maximum allowable gas pressure for an underground gas storage salt cavern – A case study of Jintan, China. *Journal of Rock Mechanics and Geotechnical Engineering*, *11*, 251–262. doi: 10.1016/j.jrmge.2018.10.004

Wang, T., Yan, X., Yang, H., Yang, X., Jiang, T., & Zhao, S. (2013, April). A new shape design method of salt cavern used as underground gas storage. *Applied Energy*, *104*, 50–61. doi: 10.1016/j.apenergy.2012.11.037

Wang, T., Yang, C., Ma, H., Yang, J., & Daemen, J. (2015, April). Safety evaluation of caverns for gas storage in bedded rock salt formation located close to a tectonic fault. In *Proceedings of the solution mining research institute spring 2015 technical conference.* Rochester, New York, USA. (27–28)

Warwick, N. J., Archibald, A. T., Griffiths, P. T., Keeble, J., O'Connor, F. M., Pyle, J. A., & Shine, K. P. (2023, October). Atmospheric composition and climate impacts of a future hydrogen economy. *Atmospheric Chemistry and Physics*, *23*(20), 13451–13467. Retrieved 2023-11-20, from https://acp.copernicus.org/articles/23/13451/2023/ (Publisher:

Copernicus GmbH) doi: 10.5194/acp-23-13451-2023

Wawersik, W. R., & Zeuch, D. H. (1986, January). Modeling and mechanistic interpretation of creep of rock salt below 200°C. *Tectonophysics*, *121*(2), 125–152. Retrieved 2023-10-29, from https://www.sciencedirect.com/science/article/pii/0040195186900405 doi: 10.1016/0040-1951(86)90040-5

Williams, J. D., Williamson, J., Parkes, D., Evans, D. J., Kirk, K. L., Sunny, N., ... Akhurst, M. C. (2022, September). Does the United Kingdom have sufficient geological storage capacity to support a hydrogen economy? Estimating the salt cavern storage potential of bedded halite formations. *Journal of Energy Storage*, *53*, 105109. Retrieved 2022-12-03, from https://linkinghub.elsevier.com/retrieve/pii/S2352152X22011100 doi: 10.1016/j.est.2022.105109

Zheng, Y., Wanyan, Q., Qiu, X., Kou, Y., Ran, L., Lai, X., & Wu, S. (2020, February). New technologies for site selection and evaluation of salt-cavern underground gas storages. *Natural Gas Industry B*, *7*(1), 40–48. Retrieved 2022-01-20, from https://www.sciencedirect.com/science/article/pii/S2352854020300061 doi: 10.1016/j.ngib.2019.06.002

Zhu, S., Shi, X., Yang, C., Li, Y., Li, H., Yang, K., ... Liu, X. (2023). Hydrogen loss of salt cavern hydrogen storage. *Renewable Energy*, *218*, 119267.

Zivar, D., Kumar, S., & Foroozesh, J. (2021, July). Underground hydrogen storage: A comprehensive review. *International Journal of Hydrogen Energy*, *46*(45), 23436–23462. Retrieved 2021-10-20, from https://www.sciencedirect.com/science/article/pii/S0360319920331426 doi: 10.1016/j.ijhydene.2020.08.138

Ślizowski, J., Lankof, L., Urbańczyk, K., & Serbin, K. (2017, July). Potential capacity of gas storage caverns in rock salt bedded deposits in Poland. *Journal of Natural Gas Science and Engineering*, *43*, 167–178. Retrieved 2022-03-02, from https://www.sciencedirect.com/science/article/pii/S1875510017301476 doi: 10.1016/j.jngse.2017.03.028